Appl. Phys. B (2014) 116:7–13
DOI 10.1007/s00340-014-5845-7

Applied Physics B
Lasers and Optics

RAPID COMMUNICATION

Femtosecond two-photon LIF imaging of atomic species using a frequency-quadrupled Ti:sapphire laser

Waruna D. Kulatilaka · James R. Gord · Sukesh Roy

Received: 26 February 2014 / Accepted: 13 April 2014 / Published online: 29 April 2014

Abstract Femtosecond (fs)-duration laser pulses are well suited for two-photon laser-induced-fluorescence (TPLIF) imaging of key atomic species such as H, N, and O in gas-phase reacting flows. Ultrashort pulses enable efficient nonlinear excitation, while reducing interfering photochemical processes. Furthermore, amplified fs lasers enable high-repetition-rate imaging (typically 1–10 kHz) for capturing the dynamics of turbulent flow fields. However, two-dimensional (2D), single-laser-shot fs-TPLIF imaging of the above species is challenging in most practical flow fields because of the limited ultraviolet pulse energy available in commercial optical parametric amplifier (OPA)-based tunable laser sources. In this work, we report the development of an efficient, fs frequency-quadrupling unit [i.e., fourth-harmonic generator (FHG)] with overall conversion efficiency more than six times greater than that of commercial OPA-based systems. The development, characterization, and application of the fs-FHG system for 2D imaging of H atoms in flames are described in detail. The potential application of the same laser system for 2D imaging of N and O atoms is also discussed.

1 Introduction

Highly reactive intermediate atomic species, such as atomic hydrogen (H), atomic oxygen (O), and atomic nitrogen (N), play critical roles in numerous chain-branching reactions in hydrocarbon combustion as well as various nonequilibrium-plasma applications. Spatially and temporally resolved quantitative concentration measurements of these species are extremely important for increasing fundamental understanding of the physical and chemical processes taking place in such systems as well as for developing model-based predictive capabilities. Tunable radiation at deep-ultraviolet (UV) frequencies near 200 nm, particularly in the ultrashort-pulse regime [picosecond (ps) and femtosecond (fs) duration] is required for a variety of spectroscopic techniques involving those measurements [1–8]. For example, two-photon excitation of species such as H (2×205 nm) and N (2×207 nm) requires high-power UV beams, particularly when techniques such as two-photon planar laser-induced fluorescence (TPLIF) are used for diagnostic applications in gas-phase reaction media [1, 3]. In such systems, we demonstrated previously that fs-duration pulses have significant advantages as compared to nanosecond (ns)- or ps-duration pulses [1]. Utilization of low energy but high-peak-power ultrashort pulses results in efficient two-photon excitation, while minimizing photodissociation processes in the medium that can generate the same species as those being probed [1–3, 5].

However, generating sufficiently intense ultrashort-pulse radiation near 200 nm from amplified Ti:sapphire lasers has been challenging, primarily because of the limited availability of suitable nonlinear optical crystals, particularly for deep-UV applications. Beta-barium-borate (BBO) crystals are best suited, and, hence, commonly used for such frequency-conversion processes because of their high nonlinear crosssection, high optical-damage threshold, and broad transparency range [10–12]. However, for frequency-quadrupling the ~800-nm fundamental output of

W. D. Kulatilaka (✉) · S. Roy
Spectral Energies, LLC, 5100 Springfield Street, Suite 301, Dayton, OH 45431, USA
e-mail: waruna.kulatilaka.1.ctr@us.af.mil

J. R. Gord
Air Force Research Laboratory, Aerospace Systems Directorate, Wright-Patterson Air Force Base, OH 45433, USA

amplified Ti:sapphire lasers, the second-doubling stage requires near-cutoff BBO phase-matching angles (i.e., 86° for frequency-doubling 400-nm radiation to 200 nm) [13]. A more commonly used scheme is second-harmonic generation (SHG) of the fundamental followed by third-harmonic generation (THG) and subsequent mixing with the fundamental for fourth-harmonic generation (FHG) to obtain the required UV wavelengths [8, 13]. For applications requiring wider wavelength tuning, a common practice is the use of optical parametric amplification (OPA) followed by subsequent frequency-doubling and mixing stages. However, when the energy per pulse is considered, the overall conversion efficiencies of both of these types of commercially available systems are generally well below 1 % at ~200 nm; hence, they do not produce sufficient UV energy for high-temperature gas-phase imaging applications such as TPLIF of H and N [1].

In the present work, we utilized a home-built fs-FHG system that has an overall per-pulse conversion efficiency of nearly 2 % around 200 nm for two-dimensional (2D), 10-kHz fs-TPLIF imaging of H atoms in flames. The current scheme employs an SHG and a THG stage in series followed by a mixing stage of the third harmonic with the fundamental. As compared to many such systems that have been developed in the past [8], the current scheme utilizes collinear frequency-doubling (i.e., SHG) and frequency-tripling (i.e., THG) stages with inter-stage delay compensation. The design and characteristics of this system are described in the next section. As a potential application of this system, we demonstrate single-laser-shot 1D (one-dimensional) and 2D fs-TPLIF imaging of H in flames at 10 kHz. Such high-repetition-rate imaging capabilities are vital for understanding dynamics of turbulent combustion, such as localized flame extinction and reignition in fundamental laboratory flames as well as modern lean burn, low-NOx combustion devices [14]. The potential for utilizing the current fs-FHG system for TPLIF imaging of N (2 × 207 nm), O (2 × 201 nm), and Kr (2 × 204 nm) is also discussed.

2 Experimental

The schematic of the fs-FHG system is shown in Fig. 1. To generate UV radiation, the fundamental output of the regenerative amplifier was directly frequency quadrupled. The input-beam energy was ~1 mJ/pulse at 10 kHz. It should also be noted that the same pump laser is capable of operating at either 5 or 1 kHz (with minor modifications), thereby increasing the pulse energy to 2 mJ or 10 mJ/pulse, respectively. The fundamental beam was down collimated to a diameter of ~2.5 mm using a telescope with a +200 mm/−50 mm lens combination. The telescope was

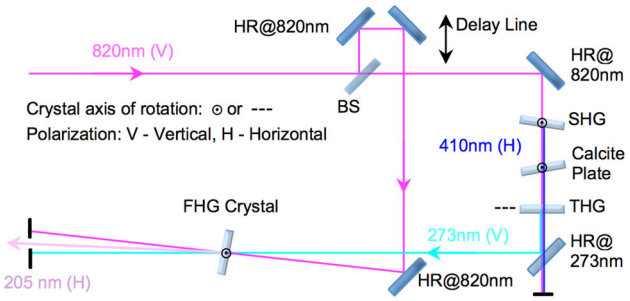

Fig. 1 Schematic of the fs-FHG apparatus. HR—high reflector, BS—beamsplitter

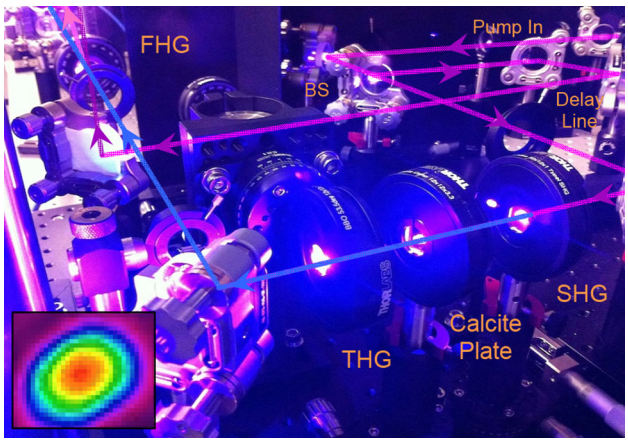

Fig. 2 Photograph of the fs-FHG system in operation. Shown on the *bottom*, *left-hand* corner is a typical beam profile of the UV output at a distance of 1 m from the FHG crystal

adjusted to peak up the FHG output energy, resulting in a slightly expanded output beam of ~4 mm diameter. Approximately, 30 % of the fundamental beam was split-off and sent through a delay line to be used in the final mixing stage. The BBO crystals used in the SHG, THG, and FHG stages were 1.0, 1.0, and 0.4 mm thick and were cut at phase-matching angles of 28.5°, 42.8°, and 61.3°, respectively. A 3.3-mm-thick calcite compensator plate was used after the SHG stage to compensate for the delay between the second- and THG processes. The calcite plate was angle tuned for fine adjustment of the delays, thereby optimizing the THG efficiency. The third-harmonic beam was crossed with the portion of the fresh fundamental beam at an angle of ~2° in the final mixing stage. The motorized delay stage that controlled the temporal overlap of the pulses had a linear accuracy <1 μm. The generated fourth-harmonic UV beam emerged between the two input beams, closer to the third-harmonic beam, as depicted by the phase-matching condition. The complete system was assembled on a 2-ft × 3-ft optical breadboard. The system in operation, along with a typical beam profile of the UV

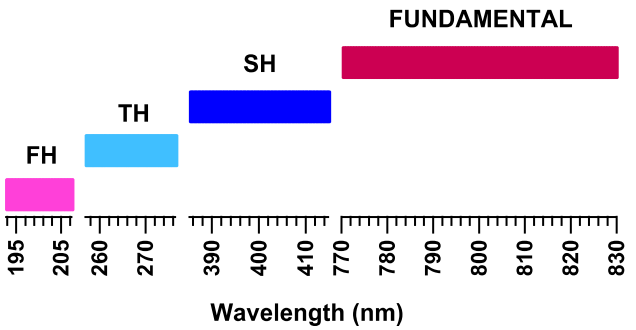

Fig. 3 Wavelengths covered by the fundamental and harmonics of the fs-FHG apparatus

output recorded at 200 nm, is shown in Fig. 2. This beam profile was recorded using a UV converter attached to a beam-profiling camera system.

Wavelength tunability of the FHG output beam was achieved by changing the fundamental wavelength of the pump laser. Although the wavelength of the modelocked Ti:sapphire seed laser can be tuned widely, the tunability range of the regeneratively amplified output beam is limited, in part because of the "gain-pulling" effect at the Ti:sapphire gain peak near 800 nm. As a result, the seed wavelength had to be set to ~840 nm for the regen cavity to lase at 820 nm. Furthermore, the optics in the pulse stretcher and the amplifier are optimized for ~800-nm operation and, hence, may not have the optimum reflectivity needed for operating at detuned wavelengths, which would reduce the overall output power at such wavelengths. Shown in Fig. 3 is the wavelength range achievable by tuning the fundamental between 770 and 830 nm while maintaining the power drop at <10 %, as specified by the laser manufacturer. The corresponding wavelength ranges of the different harmonics of the FHG system. For this tuning range, fourth-harmonic wavelengths of ~193–207 nm could be achieved with average pulse energy >16 μJ/pulse when pumping with 1 mJ/pulse of the fundamental beam. Hence, this system can be used effectively for typical two-photon excitation of atomic species such as H, N, O, and Kr, as outlined above. We have experimentally verified the tunability of the UV output up to 207 nm, and N and Kr imaging has been performed. Those measurements will be reported in forthcoming publications.

The fs-FHG system described above was used for proof-of-principle 2D imaging of H in flames using TPLIF. The fs-TPLIF scheme and the burner facility are described in detail in our earlier paper [1]; however, in that work, we used a commercially available OPA system to generate 205-nm radiation for two-photon excitation. In the present work, we employed the high-energy UV pulses generated with the fs-FHG system described above to extend those measurements to full 2D imaging and, hence, to explore the full potential of the fs-FHG system developed in-house. A brief description of the flame experiment is given below. We used 205-nm radiation for two-photon excitation of the $n = 1 \rightarrow\rightarrow n = 3$ transition, and the subsequent H_α fluorescence at 656 nm from the $n = 3 \rightarrow n = 2$ decay was detected. A 5-mm-diameter underexpanded jet was employed to generate a $CH_4/O_2/N_2$ Bunsen flame with a flame height of ~15 mm. The burner was operated at slightly fuel-rich conditions at a flame equivalence ratio (ϕ of 1.2). When needed, a piston-based pulsating unit was added to the premixed-gas line, thereby generating driven flames at a desired frequency, which resulted in well-characterized dynamic flame conditions. The 205-nm output beam from the FHG unit had a beam diameter of ~4 mm and was subsequently formed into a laser sheet above the measurement volume of the Bunsen flame using a $f = +200$-mm cylindrical lens. A dual-stage high-speed intensifier (LaVision High Speed IRO with S25 visible-enhanced photocathode) coupled to a complementary metal-oxide-semiconductor (CMOS) camera system (Photron FastCAM SA-X) was employed for imaging the H-atom fluorescence signal. A 656 ± 40-nm bandpass filter was used in front of the camera lens to suppress the scattered light and flame emission. The active image region was limited to the middle part of the camera frame (~500 × 500-pixel region out of 1,024 × 1,024-pixel array) where uniform spatial response was verified during previous studies [1].

3 Results and discussion

3.1 Performance characterization of fs-FHG system

Performance of the FHG system was characterized in terms of the frequency bandwidth, temporal pulse width, conversion efficiency, and spatial beam quality, while pumping at 800 nm. The frequency spectra of the laser pulses at each stage were recorded using a fiber-coupled spectrometer having a spectral resolution of 0.2 nm (Ocean Optics USB 4000); these spectra are shown in Fig. 4. The typical temporal width of the optimally compressed fundamental output from the regenerative amplifier was in the range 80–100 fs, as measured by a home-built autocorrelator as well as a commercial single-shot autocorrelator (Coherent SSA). However, the pulse compressor of the pump laser had to be detuned from the peak to optimize the FHG output energy, thereby compensating for the frequency chirp within the optical elements in the system. The pulse width of the third harmonic was measured by crosscorrelating with the pump beam, for which the existing delay line and the FHG crystal were used directly. To measure

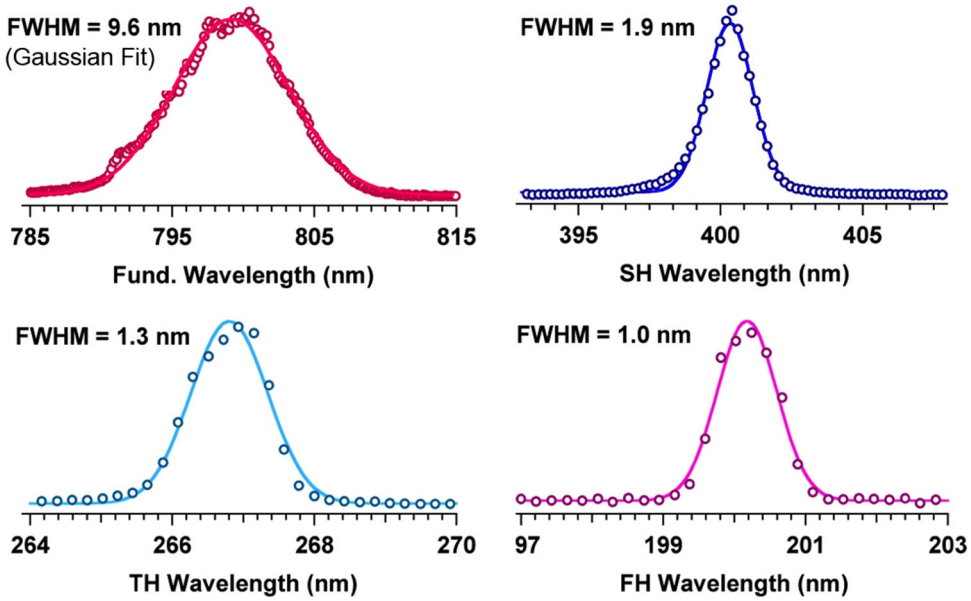

Fig. 4 Spectral bandwidths of the fundamental and harmonics of the fs-FHG system

Table 1 Measured pulse characteristics of the fundamental and harmonics at optimal FH output energy

Beam/ parameter	Conversion efficiency (%)	Pulse width (fs)	Bandwidth (nm)	TBP
Fund (800 nm)	–	170	9.6	0.76
SH (400 nm)	21	–	1.9	–
TH (267 nm)	28	175	1.3	0.96
FH (200 nm)	41	270	1.0	2.02

The 800-nm pulse energy was ~1 mJ/pulse. The time-bandwidth product (TBP) for transform-limited (TL) Gaussian pulses is 0.441. Pulse widths reported are Gaussian widths. Pulse width of the second-harmonic output was not measured

the pulse width of the fourth-harmonic beam, a difference-frequency-generation (DFG) scheme was established. A portion of the pump pulse ($\lambda = 800$ nm) was sent through a delay line and mixed with the fourth-harmonic output ($\lambda = 200$ nm) in a 0.2-mm-thick Type-I BBO crystal ($\theta = 61.4°$) to generate the DFG beam at 266 nm. The delay of the 800-nm beam was scanned to obtain the DFG crosscorrelation trace. The resulting pulse characteristics are summarized in Table 1. The frequency-conversion efficiencies of each crystal stage were also measured by reflecting the second-harmonic and third-harmonic outputs using three dichroic mirrors at corresponding wavelengths, thereby completely dumping the residual input beams at each stage. These results are also included in Table 1. Pulse width of the second-harmonic output was not measured.

In the present configuration, we observed substantial spectral narrowing and a time-bandwidth product (TBP) of ~2 at the fourth-harmonic wavelength. In this case, the system was operated to obtain the maximum fourth-harmonic output-pulse energy and, hence, was not optimized for the shortest possible pulse width. Several potential techniques exist for improving the TBP; these include optimizing the beam-focusing conditions [15], implementing phase-correction dispersive gratings [16], and employing output pulse-compression methods such as a simple pulse compressor or a more precise multiphoton-intrapulse-interference phase-scan (MIIPS) scheme [17]. However, the benefits of employing such schemes must be weighed against the significant intensity losses associated with the low-transmission-efficiency UV optics in such systems.

The present system has excellent wavelength stability with no observable wavelength drift over a period of several hours of operation, provided the pump laser operates in a stable fashion. The average pulse energy of the pump laser monitored over a period of 2 h was 1.163 mJ/pulse with 0.45 % standard deviation, while the corresponding average fourth-harmonic output was 16 μJ/pulse with 3.8 % standard deviation. We also changed the repetition rate of the pump laser from 10 to 5 kHz, while maintaining the overall output power nearly unchanged and increasing the corresponding fourth-harmonic output energy to ~32 μJ/pulse. Similarly, if the same regenerative amplifier is operated at 1 kHz—which is achievable with slight modifications to the optics inside—the pump pulse energy can be increased tenfold, and fourth-harmonic UV pulse energies in excess of 150 μJ/pulse are expected from the current system. Such pulse-energy levels will be almost a factor-of-40 improvement over past FHG systems reported in the literature [8]. Furthermore, the beams are not tightly focused in the current configuration, leaving a substantial buffer over the optical-damage intensity of the crystal

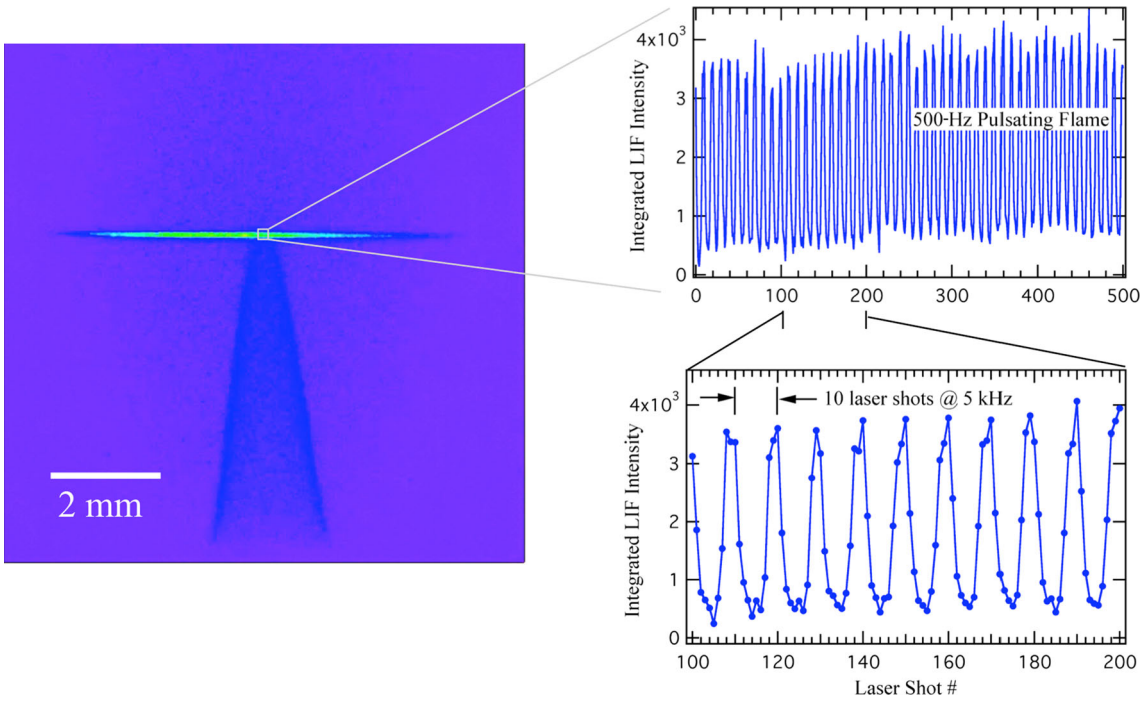

Fig. 5 Fs-TPLIF imaging of H in a pulsating flame. The integrated fluorescence signal in a 4-pixel × 4-pixel (i.e., 80 μm × 80 μm) area is also plotted for each frame recorded at 5 kHz. The plot on the *lower right* shows an expanded view of the integrated LIF signal over 100 consecutive laser pulses

material. Therefore, it is expected that the system will operate at similar or even higher conversion efficiency if a higher power pump laser is available. To increase the conversion efficiency further, beams may be focused more tightly using nondispersive optics such as curved mirrors without adding additional frequency chirp and perhaps even improving the TBP as described above [15]. Furthermore, it may be possible to improve the efficiency of the final mixing stage by adding additional dispersive material to match the pulse width of the split-off fundamental beam to that of the third-harmonic beam. Such configurations will be explored during future refinements of the fs-FHG system.

3.2 TPLIF imaging of H using the fs-FHG system

The successful operation of the fs-FHG system was demonstrated in H fs-TPLIF imaging. As described above, the experimental configuration is very similar to that of our previous work, where photolytic-interference-free H-atom line imaging was performed using fs pulses generated using a commercial OPA unit [1]. In the present work, the low-efficiency, OPA-based, 205-nm generation scheme was replaced by the new fs-FHG scheme by tuning the fundamental to 820 nm. Initially, H-atom line images were recorded at the tip of a pulsating $CH_4/O_2/N_2$ flame (equivalence ratio, $\Phi = 1.2$) that was driven at a fixed frequency of 500 Hz, as shown in Fig. 5. In this particular set of experiments, the fs amplifier was operated at 5 kHz, thereby generating FHG output energy of ~32 mJ/pulse. It should be noted that this operating condition resulted in peak TPLIF signals of H, although the overall FHG conversion efficiency was lower than that reported in Table 1. We attribute this behavior to increased frequency chirp introduced, while operating the system at the peak power, as described above. As described in detail in Ref. [1], the H-atom signals recorded here are free from interferences that would have resulted from photolytic breakdown of hydrogen-containing species in the medium if high-power ns- or ps-duration laser pulses had been used. The potential to make such measurements at data rates up to 10 kHz is critically important when investigating the dynamics of turbulent flames, both under laboratory conditions and in practical engine applications where thermo-acoustic flame instabilities, such as low-frequency rumble and high-frequency screech in gas-turbine augmentors, dominate.

The higher UV pulse energies available from the current FHG system enabled us to make single-laser-shot 2D H-atom images at 10 kHz using a laser sheet as high as 2 mm in the same flame described above. For these demonstration measurements, we used an aperture in the beam to select only the middle portion of the laser sheet having nearly uniform intensity distribution. A representative 2D H-atom TPLIF image recoded at 10-kHz repetition rate is

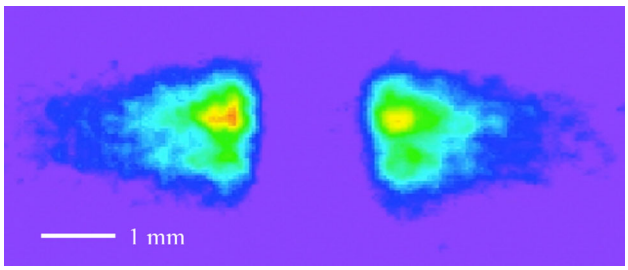

Fig. 6 Single-laser-shot 2D image of H recorded in the laminar premixed Bunsen flame using the output of the fs-FHG unit

shown in Fig. 6. In this flame, the peak H-atom number density is expected to be in the range 5×10^{16} cm^{-3} and the signal-to-noise ratio in the corresponding region is better than 30. With the approximate factor-of-10 increase in laser pulse energy that may result from the planned modifications to the laser system described earlier (i.e., 1-kHz operation as compared to 10-kHz operation), we expect to capture high-repetition-rate 2D images of H atoms in a probe region as high as 25 mm in the future.

3.3 Other TPLIF imaging applications using the fs-FHG system

As shown in these proof-of-principle fs-FHG results, the availability of high-power, high-intensity UV radiation in the 193–207-nm region is opening up a complete array of new imaging diagnostic capabilities for combustion and plasma flow applications. For example, our group is now pursuing a fundamental study of nanosecond-pulsed, low-temperature nonequilibrium plasmas where spatially resolved imaging of key intermediate species such as H, N, and O is realized through this fs-FHG system [18]. While the detailed description of such results is beyond the scope of this paper and will be discussed in future publications, it should be noted that such high-fidelity imaging measurements can easily be realized using this fs-FHG system. In addition, TPLIF imaging of inert gas species such as Kr has been used for mixture-fraction and scalar-dissipation imaging in turbulent jets and supersonic flow streams [19]. In such applications, the high-power UV output from the fs-FHG system described here can be utilized very effectively for fs-TPLIF imaging of Kr. Further experiments are also planned to implement similar imaging diagnostics in plasma-assisted combustion environments via a fs-TPLIF scheme making use of our fs-FHG system.

4 Summary

In summary, we have developed a compact, more efficient, fs frequency-quadrupling system that enables generation of tunable UV pulses near 200 nm. The utilization of this system for fs two-photon excitation of atomic species was demonstrated via 1D and 2D TPLIF imaging of H in flames. Such imaging capabilities are a significant step forward in advancing state-of-the-art nonintrusive diagnostic techniques in flames and plasmas. Furthermore, other species of interest such as N, O, and Kr can be probed via fs-TPLIF using this tunable fs-FHG system. Such measurements and extended applications in detailed combustion and plasma studies are currently underway in our laboratory.

Acknowledgments Funding for this research was provided by the United States Air Force Research Laboratory under Contract No. FA8650-12-C-2200 and by the United States Air Force Office of Scientific Research (Dr. Enrique Parra, Program Manager).

References

1. W.D. Kulatilaka, J.R. Gord, V.R. Katta, S. Roy, Photolytic-interference-free, femtosecond two-photon fluorescence imaging of atomic hydrogen. Opt. Lett. **37**, 3051–3053 (2012)
2. W.D. Kulatilaka, B.D. Patterson, J.H. Frank, T.B. Settersten, Comparison of nanosecond and picosecond excitation for interference-free two-photon laser-induced fluorescence detection of atomic hydrogen in flames. Appl. Opt. **47**, 4672–4683 (2008)
3. W.D. Kulatilaka, J.H. Frank, B.D. Patterson, T.B. Settersten, Analysis of 205-nm photolytic production of atomic hydrogen in methane flames. Appl. Phys. B **97**, 227–242 (2009)
4. W.D. Kulatilaka, J.H. Frank, T.B. Settersten, Interference-free two-photon LIF imaging of atomic hydrogen in flames using picosecond excitation. Proc. Combust. Inst. **32**, 955–962 (2009)
5. J.H. Frank, X. Chen, B.D. Patterson, T.B. Settersten, Comparison of nanosecond and picosecond excitation for two-photon laser-induced fluorescence imaging of atomic oxygen in flames. Appl. Opt. **43**, 2588–2597 (2004)
6. C. Brackmann, J. Sjöholm, J. Rosell, M. Richter, J. Bood, M. Aldén, Picosecond excitation for reduction of photolytic effects in two-photon laser-induced fluorescence of CO. Proc. Combust. Inst. **34**, 3541–3548 (2013)
7. W.D. Kulatilaka, R.P. Lucht, S. Roy, J.R. Gord, T.B. Settersten, Detection of atomic hydrogen in flames using picosecond two-color two-photon-resonant six-wave-mixing spectroscopy. Appl. Opt. **46**, 3921–3927 (2007)
8. J. Ringling, O. Kittelmann, F. Noack, G. Korn, J. Squier, Tunable femtosecond pulses in the near vacuum ultraviolet generated by frequency conversion of amplified Ti:sapphire laser pulses. Opt. Lett. **18**, 2035–2037 (1993)
9. E. Peters, S.A. Diddams, P. Fendel, S. Reinhardt, T.W. Hänsch, T. Udem, A deep-UV optical frequency comb at 205 nm. Opt. Express **17**, 9183–9190 (2009)
10. A. Dubietis, G. Tamošauskas, A. Varanavičius, G. Valiulis, Two-photon absorbing properties of ultraviolet phase-matchable crystals at 264 and 211 nm. Appl. Opt. **39**, 2437–2440 (2000)
11. K. Kato, Second-harmonic generation to 2048 A in β-BaB2O4, IEEE J. Quant. Elect. QE-22, 1013–1014 (1986)
12. J. Zhu, W. Ling, Z. Wang, P. Wang, J. Sun, Z. Wei, D. Zhang, X. Ma, W. Zhan, High-energy picosecond near-vacuum ultraviolet pulses generated by sum-frequency mixing of an amplified Ti:sapphire laser. Appl. Opt. **46**, 6228–6231 (2007)
13. F. Rotermund, V. Petrov, Generation of the fourth harmonic of a femtosecond Ti:sapphire laser. Opt. Lett. **23**, 1040–1042 (1998)

14. S. Roy, J.R. Gord, A.K. Patnaik, Recent advances in coherent anti-Stokes Raman scattering spectroscopy: fundamental developments and applications in reacting flows. Prog. Energy Combust. Sci. **36**, 280–306 (2010)
15. M.T. Reiten, R.A. Cheville, N.J. Halas, Phase matching and focusing effects in noncollinear sum frequency mixing in the near VUV region. Opt. Commun. **110**, 645–650 (1994)
16. C. Zhou, T. Kanai, X. Wang, Y. Zhu, C. Chen, S. Watanabe, Generation of ultrashort 25-μJ pulses at 200 nm by dual broadband frequency doubling with a thin $KBe_2BO_3F_2$ crystal. Opt. Express **20**, 13684–13691 (2012)
17. V.V. Lozovoy, I. Pastirk, M. Dantus, Multiphoton intrapulse interference IV: ultrashort laser pulse spectral phase characterization and compensation. Opt. Lett. **29**, 775–777 (2004)
18. H.F. Döbele, T. Mosbach, K. Niemi, V. Schulz-von der Gathen, Laser-induced fluorescence measurements of absolute atomic densities: concepts and limitations. Plasma Sources Sci. Technol. **14**, S31–S41 (2005)
19. V. Narayanaswamy, R. Burns, N.T. Clemens, Kr-PLIF for scalar imaging in supersonic flows. Opt. Lett. **36**, 4185–4187 (2011)